Flow, Turbulence and Combustion (2026) 116:56
https://doi.org/10.1007/s10494-026-00752-0

RESEARCH

On the Relation Between Presumed FDF, Subgrid Variance and Flame Speed in the Wrinkled Flamelet Regime: An *A Posteriori* Analysis

Ivan Langella[1] · **Nguyen Anh Khoa Doan**[1,2]

Received: 22 August 2025 / Revised: 9 April 2026 / Accepted: 15 April 2026

Abstract
Presumed PDF/FDF approaches with dependency on second order moments of an appropriately defined progress variable are often used in combustion modelling, but they fail in predicting the limiting behaviour of burning speed when the latter approaches the laminar condition. In this work, we discuss a recently proposed correction for the burning speed in the context of presumed FDF approaches, and test its performance using large eddy simulation (LES). First, the correction model is discussed in relation to the interlink between filtered density function and second order moment (SGS variance in the LES case) from a theoretical point of view, and the further interlink with the LES filter size is discussed. In a second step, a propane flame in the wrinkled flamelet regime of the Borghi diagram is simulated *a posteriori* using two LES filter size resolutions. We firstly show that the increase of filter size leads to an overestimation of the burning speed. We then show how the incorrect estimation of burning speed with increasing filter size is corrected and how the correction affects the SGS variance. An extended correction model for partially-premixed combustion is also proposed.

Keywords Presumed FDF · Large eddy simulation · Premixed combustion · Flame speed

1 Introduction

Computational fluid dynamics is increasingly used in academia and industry to complement experiments in the analysis of turbulent reacting flows. Large eddy simulation (LES) in particular has the potential to accurately predict time-dependent phenomena at a reasonable cost. In a LES, turbulent scales are resolved down to a cut-off scale, Δ, with models to

✉ Ivan Langella
i.langella@tudelft.nl

[1] Faculty of Aerospace Engineering, Delft University of Technology, Kluyverweg 1, Delft, HS 2629, Netherlands

[2] Faculty of Engineering, Imperial, South Kensington, London SW7 2AZ, UK

Published online: 26 May 2026

represent the residual scales (Pope 2000). Since the flame thickness is usually smaller than Δ in practical LES, the turbulent combustion process needs to be modelled at this residual level. Many different approaches have been proposed in the past for this interaction, which can be broadly categorised into flamelet and non-flamelet, or geometrical and statistical approaches (Gicquel et al. 2012).

The focus in this work is on presumed-FDF approaches with an unstrained flamelet database. In the LES context, the presumed filtered density function (FDF) takes the place of the fine grained probability density function (PDF), and is often parametrised with first and second order (Favre-filtered) moments of the progress variable. The FDF statistically represents subgrid scale (SGS) processes such as flame oscillations and wrinkling. An often used presumed shape with dependency of first and second order moments is the β function, which has shown good accuracy at various regimes of the Borghi diagram at least for $\Delta \leq \delta_{th}$, e.g. see Klapdor et al. (2013); Trisjono et al. (2014); van Oijen et al. (2014); Donini et al. (2017); Galeazzo et al. (2019). Alternative approaches are the sum of Dirac δ-functions (Ribert et al. 2004), the laminar flamelet PDF (Salehi et al. 2013; Bray 2016), or analytical forms (Pfitzner 2021). These were shown to perform better in the case of flame intermittency and coarser meshes with $\Delta > \delta_{th}$ (Salehi and Bushe 2010; Lecocq et al. 2011), and have the advantage of not relying on second order moments (Lipatnikov et al. 2021). The less accurate performance of the β function at regimes of strong intermittency (e.g. flamelet regime) and at $\Delta > \delta_{th}$ is associated to its intrinsic dependence on the second order moment and, in the case of LES, to the filter size, as will be discussed in Sect. 3. This dependency can be circumvented in the LES by enforcing a physical constraint on the burning speed. A model for LES in this sense was recently tested a priori by 27, and is tested here *a posteriori*. This correction is also discussed in this paper in the context of the interlink between FDF and SGS variance and is extended for partially premixed combustion. It will be shown that this extension is independent of fuel, initial conditions, and easy to implement in CFD codes.

The quasi-laminar premixed flame configuration studied experimentally by 9 is chosen for the *a posteriori* assessment, since this flame lies in the wrinkled reaction zone regime of the Borghi diagram where the β function used to represent the FDF is expected to lead to over-prediction of the flame speed. Two base cases LES are first performed on two meshes to mimic the effect of the increasing filter size, proving the over-prediction of flame speed when $\Delta > \delta_{th}$ and consequent shortening of the flame. A further simulation on the coarser mesh is then performed using the flame speed correction model to evaluate its effectiveness, and the interlink with the SGS variance is discussed.

2 LES Methodology

2.1 Presumed FDF Approach

A presumed FDF approach with unstrained flamelet database is employed to close the subgrid turbulence-combustion interaction in the LES. A priori analyses of the various modelling elements within this approach were performed in previous studies (Doan et al. 2017; Langella et al. 2018, Nilsson et al.,2019a, 2019b). Effects on the reaction rate of strain at SGS level are neglected due to the ability of the LES to resolve most of the strain at least away from blow-off (Langella and Swaminathan 2016; Doan et al. 2017; Soli et al. 2022).

The flamelet assumption assumes the flame to be thin enough so that small eddies wrinkle but do not modify its inner structure. The thermochemistry can thus be computed a priori and linked to the LES by tracking the reaction progress. In this work, this is done by defining a scaled progress variable as $c = \Psi/\Psi^b$, where $\Psi = Y_{\mathrm{CO}_2} + Y_{\mathrm{CO}}$, Y_k is the mass fraction of species k, and Ψ^b is the equilibrium value of Ψ. The choice of this definition is based on previous works (Fiorina et al. 2003, Langella et al. 2016). The transport equation for the filtered progress variable $\widetilde{c}$ is

$$\overline{\rho}\frac{D\widetilde{c}}{Dt} = \nabla \cdot \left[\left(\overline{\rho\mathcal{D}} + \frac{\mu_t}{Sc_t}\right)\nabla\widetilde{c}\right] + \overline{\dot{\omega}}_c \tag{1}$$

where D/Dt refers to the total derivative, $\overline{\rho D} \approx \mu/\mathrm{Sc}$ is the filtered molecular diffusion term which is expressed using a gradient hypothesis in terms of dynamic viscosity μ and Schmidt number $\mathrm{Sc} = 0.7$, μ_t is the SGS viscosity, $\mathrm{Sc}_t \approx 0.7$ is the SGS Schmidt number and ρ is the mixture density. Overbars and tildas indicate simple and Favre filter operations respectively. Although counter-gradient effects may exist in the configuration described in Sect. 4.1, they are implicitly captured at resolved level in a LES and the influence of unresolved fluxes on the main solution was shown to be small in most cases (Fiorina et al. 2015). Moreover, counter-gradient effects were observed to be strong only at low Lewis numbers (Klein et al. 2016). For these reasons and the sake of simplicity, counter-gradient effects are not investigated in this work.

The filtered reaction rate of c, $\overline{\dot{\omega}}_c$ is closed as

$$\overline{\dot{\omega}}_c = \overline{\rho}\int_0^1 \frac{\dot{\omega}_c}{\rho}\,\mathcal{F}(c)\,dc \tag{2}$$

where the integrand is computed a priori for a one-dimensional, freely propagating, unstrained laminar premixed flame. The FDF is presumed using a β-function, $\mathcal{F}(c) = \beta(c; \widetilde{c}, \sigma_c^2)$. As the SGS variance of c, σ_c^2, is also the second order moment of c, the interlink between flame speed and second order moment at quasi-laminar conditions can be investigated. σ_c^2 is obtained in the LES using a transport equation:

$$\begin{aligned}\overline{\rho}\frac{D\sigma_c^2}{Dt} \approx{}& \nabla \cdot \left[\left(\overline{\rho\mathcal{D}} + \frac{\mu_t}{Sc_t}\right)\nabla\sigma_c^2\right] \\ &+ 2\,\frac{\mu_t}{Sc_t}\left(\nabla\widetilde{c}\cdot\nabla\widetilde{c}\right) + 2\left(\overline{c\,\dot{\omega}_c} - \widetilde{c}\,\overline{\dot{\omega}}_c\right) - 2\overline{\rho}\,\widetilde{\varepsilon}_c\end{aligned} \tag{3}$$

The reaction term $\mathcal{R} = \overline{c\,\dot{\omega}_c} - \widetilde{c}\,\overline{\dot{\omega}}_c$ is modelled consistently to Eq. (2). The scalar dissipation rate (SDR, last term in Eq. (3)) is closed using the model proposed by Dunstan et al. (2013), and used *a posteriori* at various regimes of the Borghi diagram, e.g. see Langella et al. (2016a,b). This model features an explicit dependence on the subgrid kinetic energy k, which is modelled using the Localised Dissipation model proposed by 18. The model constant in the SDR expression, β_c, was optimised for the particular choice of k via sensitivity analyses against experimental data, which lead to a value $\beta_c = 25$.

2.2 LES Details

The Favre-filtered transport equations for mass, momentum and absolute specific enthalpy $\widetilde{h}$ (sum of sensible, $\widetilde{h}_s$ and formation, $\widetilde{\Delta h}_f^0$, enthalpies), along with the equations for combustion described in Sect. 2.1, are solved using the low-Mach formulation of the reacting Navier-Stokes equations and the finite volume method. An additional transport equation for a passive scalar tracker, $\widetilde{Z}$, is used to take into account the effect of mixing with air on thermodynamic properties in non-reacting regions, as will be explained later. The pressure-density-velocity coupling is solved using the PISO loop implemented in OpenFOAM and 5 external loops per time step. The subgrid viscosity in the momentum equation is modelled using a one-equation model by Chai and Mahesh (2012). The turbulent fluxes in all scalar transport equations are modelled using a gradient hypothesis. The molecular dynamic viscosity is temperature dependent via Sutherland's law. The temperature is computed as $\widetilde{T} = T_0 + (\widetilde{h} - \widetilde{\Delta h}_f^0)/\widetilde{C}_p^*$, where $T_0 = 298.5\,\mathrm{K}$ and $C_p^* = (\int_{T_0}^{T} C_p\, dT\prime)/(T - T_0)$ is precomputed, C_p being the constant-pressure specific heat capacity of the mixture. This equation comes immediately by inverting $h = \Delta h_f^0 + \int_{T_0}^{T} C_p\, d\,T$ and applying the theoreom of the integral mean. The mixture density is computed from the state equation as $\overline{\rho} = \overline{p}\widetilde{W}/(R_0\widetilde{T})$, where $\overline{p}$ is the modified pressure (Pope 2000), $\widetilde{W}$ is the mixture molecular weight and R_0 is the universal gas constant. The Favre-filtered values for $\widetilde{\Delta h}_f^0$, $\widetilde{C}_p^*$ and $\widetilde{W}$ are obtained from the flamelets database using an equation consistent with Eq. (2), and then tabulated in terms of the controlling variables $\widetilde{c}$ and σ_c^2. The generic thermodynamic quantity Φ_{reac} (e.g. the specific heat capacity) from the precomputed table is weighted in the LES with the value in air as $\widetilde{\Phi} = \widetilde{Z}\Phi_{\mathrm{reac}} + (1 - \widetilde{Z})\Phi_{\mathrm{air}}$.

Second order central schemes are used for the convective terms, with TVD limiters used for the scalars to deal with steep gradients in the flame region. The flamelet database is computed using the code Chem1d developed at TU Eindhoven with detailed chemistry for propane (Kee et al. 1985), which provides computed values for laminar flame speed and laminar flame thickness of 0.34 m/s and 0.4 mm respectively. Differential diffusion effects on the reaction rate were tested for the propane/air flamelet and found to be negligible, therefore are not included. Moreover, reactions rates near the anchoring point are observed to be small due to the effect of vortex shedding in this region, therefore heat loss effects on the reaction rate are also expected to be small and are not considered in this study.

3 SGS Variance, FDF and Flame Speed Correction

The transport equation for the SGS variance σ_c^2 of a reacting progress variable c in Eq. (3) features the balance between reaction, turbulence and dissipation typical of premixed flames. The reactive term $\mathcal{R}$ in this equation vanishes for $\Delta \to 0$, but is of leading order for $\Delta = \mathcal{O}(\delta_{th})$ (Langella and Swaminathan 2016), implying that for $\Delta \geq \delta_{th}$ the variance is not zero even at laminar or quasi-laminar conditions ($\mathcal{P} = 2\mu_t(\nabla\widetilde{c} \cdot \nabla\widetilde{c})/Sc_t \approx 0$). This is because the flame is filtered out on the LES mesh and can still have subgrid oscillations, whose probability to occur is taken into account by the FDF model via a non-zero SGS variance. In this sense the FDF represents different processes than the fine-grained PDF in

RANS, which measures the probability to find a burning state at one point. Similarly, the bimodal limit is only achievable in LES at very large filter sizes, implying that the variance of c is entirely at the unresolved level. The relation between FDF and (instantaneous) SGS variance is thus not identical to that between PDF and (total mean) variance.

The significance of the SGS variance with increasing LES filter width could also be interpeted in relation to the filtered reaction rate. As Δ increases, increasingly more unburnt or burnt gases take part in the filtering operation. Since $\dot{\omega} \approx 0$ outside the flame, the filtered reaction rate has to decrease, and this decrease is enforced by increasing the SGS variance in the presumed FDF approach. However, this also implies that one would have non-zero SGS variance for filter widths larger than the laminar flame thickness, in case of steady flame. Having in mind an unstretched 1D laminar flame, in absence of SGS wrinkling one can write (Fiorina et al. 2010):

$$\int_{-\infty}^{+\infty} \overline{\dot{\omega}}\, dx = \int_{-\infty}^{+\infty} \dot{\omega}\, dx \tag{4}$$

This equation suggests that the overall burning rate before and after the filtering operation has to be preserved, or equivalently the combustion model must return the laminar flame speed. Nevertheless, as explained earlier, the SGS variance, even if the exact one from DNS is used, is not zero for large Δ even for zero-wrinkling. Thus the equality in Eq. (4) would not hold in case of a presumed-FDF approach with dependency on second-order moments. Since $\mathcal{R} \to 0$ for $\Delta \to 0$ also implies $\sigma_c^2 \to 0$ in Eq. (3) if no wrinkling is present ($\mathcal{P} = 0$), for small filter widths, Eq. (4) is implicitly verified as the β function degenerates into a δ function in this case. Consistently, it was shown by 27 that the error on the burning speed is negligible up to $\Delta = \delta_{th}$. On the other hand, imagining now the case of a wrinkled flame, for increasing Δ, the SGS variance has to increase to incorporate the physical effect of subgrid wrinkling, so Eq. (4) would not be satisfied in this case. Since the actual amount of SGS wrinkling is not known a priori in a LES, it is not possible to ensure Eq. (4) in this modelling framework. To overcome this limitation, the relation between modelled and exact consumption speeds was further analysed via DNS by Nilsson et al. (2019b), and a more general equality valid for any SGS variance was proposed:

$$\int_{-\infty}^{+\infty} \overline{\dot{\omega}}\, dx = \int_{-\infty}^{+\infty} \overline{\dot{\omega}}_e\, dx \tag{5}$$

In the above, the laminar reaction rate within the integral on the right-hand side of Eq. (4) is replaced by the 'exact' filtered reaction rate, obtained as

$$\overline{\dot{\omega}}_e = \int_{-\infty}^{+\infty} \dot{\omega}\, G(x;\Delta)\, dx \tag{6}$$

where, following 27, the implicit filter shape G is approximated with a Gaussian filter. Note that in a LES the filter is unknown and implied by subgrid model, grid spacing, numerical grid and discretization schemes (Kravchenko and Moin 2000; Pope 2000; Meyers and Sagaut 2007). The use of a Gaussian filter is a close approximation of the implicit LES filter for homogeneous and isotropic turbulence cases as discussed in (Pope 2000), and

is retained in this work for simplicity. Equation (6) is now valid also when the FDF has dependency on the second order moments. Moreover, as the volume integral in Eq. (5) is directly proportional to the consumption speed, the described correction is for the consumption speed only, and is thus not applied to the reaction term $\mathcal{R}$ in Eq. (3). Indeed, this term was observed to compare well to DNS data even at large Δ (Nilsson et al., 2019a). Further insights on the reasons for this are given in Sect. 4.3.

In *a posteriori* contexts, a correction factor can be constructed by dividing the RHS, computed via Eq. (2), by the LHS in Eq. (5). In the assumption of one-dimensional flamelet, this factor becomes:

$$f(\Delta) = \frac{\int_{-\infty}^{+\infty} \overline{\dot{\omega}}_e(Y_k, T;\, \Delta)\, dx}{\int_{-\infty}^{+\infty} \overline{\dot{\omega}}(\overline{c}, \sigma_c^2;\, \Delta)\, dx} \tag{7}$$

By combining Eqs. (5) and (7), and substituting the one-dimensional integral with a volume integral, the equation to impose in the LES becomes:

$$\int_{\mathcal{V}} \overline{\dot{\omega}}_e \, d\mathcal{V} = \int_{\mathcal{V}} f \overline{\dot{\omega}} \, d\mathcal{V} \tag{8}$$

where $\mathcal{V}$ is the local cell volume. The filter size Δ in the LES is computed in first attempt in this work as $\Delta = \mathcal{V}^{1/3}$, which is an approximation as the direction of the flame is not taken into account. However, in the unstructured grids used in this work the mesh elements are about equilateral and thus this error is neglected. As f depends only on Δ, it can be pre-computed to correct the overestimation of consumption speed one would obtain for $\Delta > \delta_{th}$ (Nilsson et al., 2019b). Since increasing filter widths imply increasing SGS variance in the LES, one can expect the reaction rate to decrease with coarsening mesh. The observed overestimations are thus explained here as the result of two competing factors: on the one hand, a larger Δ implies larger SGS variance (due to larger probability of SGS fluctuations in the presumed-PDF approach), which tends to decrease the overestimation of reaction rate; on the other hand, the integration of the reaction rate over a larger cell (as a result of a coarse mesh) ultimately yields an overestimation of the consumption speed. The latter effect is present also in RANS and is particularly relevant for finite volume approaches where the reaction rate is treated as a source term in tabulated approaches and directly multiplied by the local cell volume, thus should be taken into account even when the FDF/PDF is 'exact'.

The scaling factor $f(\Delta)$ is shown for propane/air mixture and equivalence ratio $\phi = 0.85$ in Fig. 1, as this is the condition of the flame to be analysed in Sect. 4.2. For small values of Δ and up to $\Delta/\delta_{th} \approx 1$, the value of f is near unity as one would expect. However, it quickly decreases for larger Δ values, indicating that the presumed PDF overestimates the filtered reaction rate for $\Delta/\delta_{th} > 1$. Note that the analytical expression of (7) requires $f(\Delta) \to 1$ for $\Delta \to 0$.

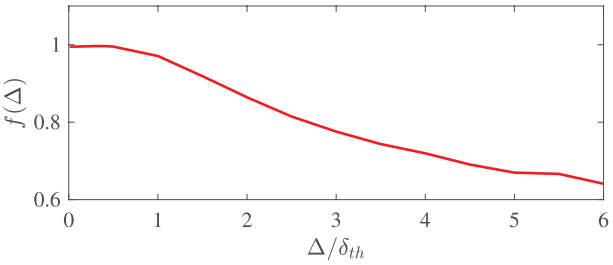

Fig. 1 Scaling factor, Eq. (7), for various values of Δ/δ_{th} for a propane/air flame at equivalence ratio $\phi = 0.85$

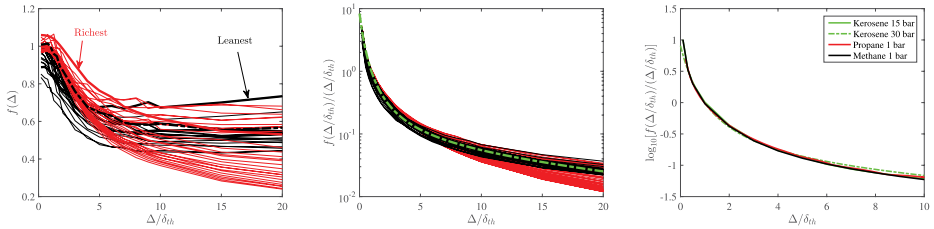

Fig. 2 Scaling function $f(\Delta/\delta_{th})$ for kerosene/air mixture at lean (—) and rich — equivalence ratios spanning the flammability limits. The stoichiometric curve is emphasised (– - –). The same curves scaled by (Δ/δ_{th}) are shown in logarithmic scale in (**b**) along with the fitting curve (– - –). The fitting curves for different fuels and pressures are shown in (**c**)

3.1 Generalised scaling

The flame speed corrector described in Sect. 3 can also be employed for partially premixed cases by computing $f(\Delta)$ for flamelets at different equivalence ratios. An example is provided in Fig. 2a. Here the values for δ_{th} are different for each flamelet, thus the actual range of Δ is different for each curve. However, the position of the peak does not change for $f(\Delta/\delta_{th})$, which is not the case for $f(\Delta)$. From this information and further scaling $f(\Delta/\delta_{th})$ by (Δ/δ_{th}) one obtains the graph in Fig. 2b, in logarithmic scale for convenience. In this scale the curves seem to have a much better collapse, which allows to look for a fitting curve in this space. Note that the scaling with (Δ/δ_{th}) does not give significant advantages in terms of percentage variation between two curves at a fixed Δ/δ_{th}, but allows to achieve a monotonic variation. Moreover, curves do not cross each other anymore if rich and lean flamelets are considered separately. The next step is to find an analytical expression to fit the function $\log_{10}(f^+)$, where $f^+ = f(\Delta/\delta_{th})/(\Delta/\delta_{th})$. By inspection of the curves, the following scaling is suggested:

$$\log_{10} f^+(x) = \frac{p_1 x^2 + p_2 x + p_3}{x + q_1} \tag{9}$$

This scaling ensures the asymptotic convergence to $f(\Delta) = 1$ for $\Delta \to 0$, and that the coefficients are of a similar order of magnitude thus avoiding possible truncation errors in the LES. The best fit is computed for the lean conditions only and found for $p_1 = -0.0253$, $p_2 = -1.373$, $p_3 = 1.354$ and $q_1 = 1.469$. The corresponding curve is shown in Fig. 2b. The same procedure is repeated for different fuels and pressures and respective fitting

curves are shown in Fig. 2c. All curves are very similar suggesting that $f^+(\Delta/\delta_{th})$ does not strongly depend on fuel and pressure and thus the same fitting curve can be used in LES under different configurations. This information suggests that the flame speed correction has a somewhat general nature, which further emphasises the arguments about filter size dependency expressed at the beginning of Sect. 3.

4 *A posteriori* Analysis

4.1 Case Study

The configuration chosen for the *a posteriori* assessment of the FDF filter width dependency described in Sect. 3 is the quasi-laminar jet flame studied experimentally by 9. This configuration lies in the wrinkled flamelet regime of the Borghi diagram where the β function is expected to overestimate the reaction rate. The experimental configuration consists of a premixed propane/air mixture issuing into a quiescent ambient at equivalence ratio $\phi = 0.85$. A direct photograph and a schematic of the flame are shown in Fig. 3. The nozzle diameter is $D = 26\,\mathrm{mm}$ and the bulk velocity in the cold flow mixture at temperature $T = 298\,\mathrm{K}$ is $U_b = 4\,\mathrm{m/s}$. As observed by Langella et al. (2016a), the burner walls are heated up by the nearby flame, causing the flow to accelerate of about 1 m/s before the nozzle exit. Also, the absence of a pilot and the relatively low speeds result in a flame sitting within the jet central region and not in the shear layer, see Fig. 3b. Consequently, the flame has a quasi-laminar behaviour due to the effect of inlet turbulence and self-induced fluctuations. For the same reason the flame remains premixed, except near the anchoring point. The numerical domain consists of the last $1.5D$ of the nozzle followed by a cylindrical region of $1\,\mathrm{m} \times 1\,\mathrm{m}$.

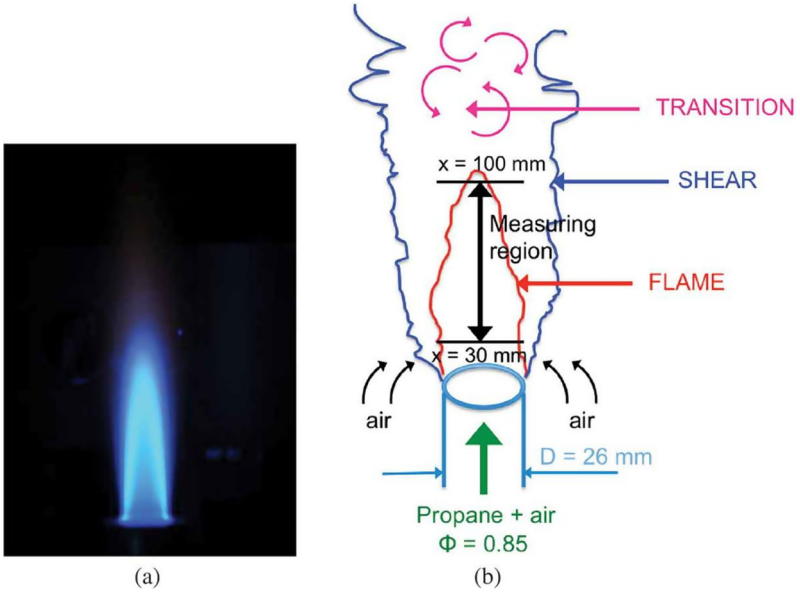

Fig. 3 Direct photograph of the premixed jet flame (**a**) and its sketch representation showing relative position of flame and shear regions (**b**). Figure taken from Langella et al. (2016b)

This domain is large enough to avoid potential numerical effects from the boundary, and is discretised using two non-structured meshes of 1 M and 6 M tetrahedral elements respectively, with refinement near the walls and the region of the flame, as shown in Fig. 4. These meshes consist of about 15 and 50 elements along the nozzle diameter respectively for the 1 M and 6 M meshes. Values of $\Delta/\delta_{th} \approx 1$ and 3 are obtained for the 6 M and 1 M meshes in the flame region, respectively. These correspond to values of about $f(\Delta) \approx 1$ and 0.75, as shown in Fig. 1. The two meshes are used to analyse the effect of the consumption speed correction in Eq. (7). As $f(\Delta) \approx 1$ in the fine mesh, the corresponding simulation provides a reference solution for the analysis to be discussed next. The coarse mesh will be used with and without the correction factor to analyse the impact of that correction factor and assess whether the correction factor can improve an initial inaccurate simulation, at least in terms of accuracy of flame speed and location.

Boundary conditions are assigned as follows. The passive tracker $\widetilde{Z}$ is assigned respectively values 1 and 0 in main jet and air coflow boundaries. The progress variable is 0 and 1 for reactant jet and entrainment inlet boundaries, respectively, while its variance is always zero on the boundary. Note that $\widetilde{c} = 1$ does not imply that burnt gases are present since the $\widetilde{Z}$ is zero here; on the contrary, this choice is optimal here as it avoids possible spurious flames in the shear layer since the region between flame and shear layer is filled by burnt gases, see Fig. 3b. A temperature of 298 K and a flat velocity profile of 0.1 m/s are assigned to the coflow boundary to mimic the entrainment. Slip-flow and zero-gradient conditions are assigned on the lateral boundaries for velocity and scalars respectively, except for the nozzle wall where a two-layer wall function model (Piomelli and Balaras 2002) is used for velocity. A zero-gradient condition is applied at the outlet for all variables except pressure, which is fixed at 1 atm. A turbulent velocity profile is assigned at the jet inlet, and the synthetic eddy method by Jarrin et al. (2006) is used to impose turbulent fluctuations with rms velocity $u\prime_{\mathrm{rms}} = 0.24\,\mathrm{m/s}$ and longitudinal and transverse integral scales respectively of $\Lambda_x = 10.9\,\mathrm{mm}$ and $\Lambda_y = \Lambda_z = 7.5\,\mathrm{mm}$ (Furukawa et al. 2016). The turbulent velocity

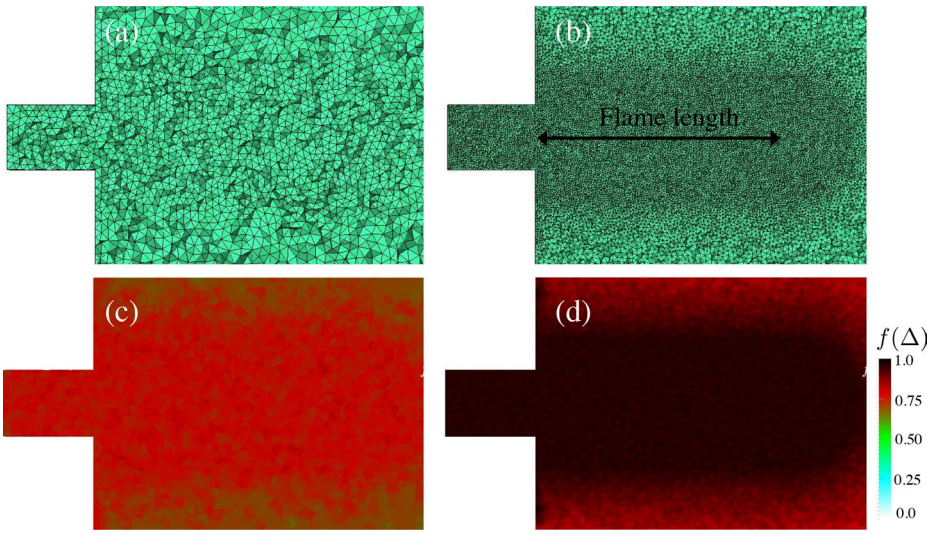

Fig. 4 Zoom of the 1 M (**a**) and 6 M (**b**) meshes used for the premixed configuration near the nozzle exit; and corresponding contours of $f(\Delta)$ (**c, d**)

profile further accounts for the effect of heat transfer at the wall as done by Langella et al. (2016b). Note that the redevelopment length as reported by Jarrin et al. (2006) (studied for channel flows) is about 3 to 4 half-heights, which is reduced as compared to other synthetic eddy approaches such as spectral or algebraic methods (Lee et al. 1992, Klein et al., 2003). Considering the length of the nozzle in the numerical domain is $1.5D$ and that the first measurement point for the case under study is about one further nozzle diameter from the jet exit, it is expected that the redevelopment distance is sufficient for the present case. A temperature profile is also used for the jet inlet accordingly. At the nozzle wall $\widetilde{T}$ is assigned to increase from 298 K to 403 K 35 mm ahead of the nozzle exit as observed experimentally. This way, heat losses to the wall are taken into account by means of wall temperature boundary conditions and inlet conditions.

The LES were performed on the Athena East Midland+ UK cluster using 196 cores. The time step of $\Delta t = 2\,\mu$s guarantees a maximum CFL number below 0.2 on both meshes. Statistics were collected for at least 6 flow-through times, τ_f, after achieving statistically steady state, where $\tau_f = L_f/U_b$ and $L_f \approx 100\,\mathrm{mm}$ is the flame length from experiments. Each simulation took about 2 days and 2.5 hours on a wall clock respectively for the 6 M and 1 M meshes.

4.2 LES Results

The flame length L_f can be inferred from the peak location of the centreline axial velocity in Fig. 5. Since incorrect flame speeds would lead to incorrect flame lengths, this velocity is used here as an indicator of the correct flame speed. Indeed, the spurious increase of consumption speed can be verified by the comparison of the numerical simulations on different grids, implying different filter widths. When using the 6 M grid the correct amount of SGS variance on the flame is achieved, leading to the correct flame length, thus the correct flame speed as observed in Fig. 5. The velocity increase near $x \approx 100\,\mathrm{mm}$ is in fact caused by the thermal dilatation from the flame tip. As expected, when switching to the 1 M mesh, the flame accelerates due to overprediction of reaction rate. The flame length, indicated by the new position of the axial velocity peak at $x \approx 45\,\mathrm{mm}$, decreases by a factor 2 and the increased heat release causes the peak velocity to increase by a factor 1.5. The strong effect of flame dilatation is also reflected in the radial rms velocity shown in Fig. 5, that is

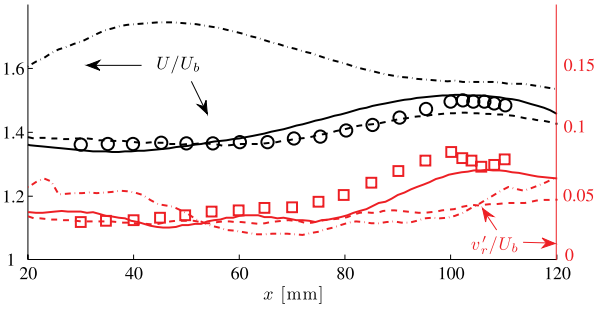

Fig. 5 Centreline variation of mean normalised axial velocity, $\langle U\rangle/U_b$ and radial rms velocity, $\sqrt{\langle v_r'\rangle}/U_b$ from measurements of Furukawa et al. (2016) (symbols) and LES for the 6 M (—) and 1 M meshes with (– –) and without (– - –) flame speed corrector. Values for U/U_b for the 1 M grid without flame speed corrector are multiplied by 0.75 to fit to the scale

observed to increase near the flame tip. For the case with the flame speed corrector, one can notice that the flame position switches back at about the right position (see dashed lines in Fig. 5). Comparisons of radial velocity rms also improve for $x < 80\,\mathrm{mm}$, however some underestimation is observed for downstream positions which could be caused by numerical diffusion due to the coarser mesh. Contours of mean temperature are shown for the two grids in Fig. 6 (top), further highlighting the better accuracy when using the corrector.

It is worth noting that additional velocity measurements were taken in 9, which showed the occurrence of a bimodal behaviour in the radial component of the velocity field across the flame at certain axial locations. Moreover, the velocity measurements were processed in the same work to construct progress variable isolines and flame brush thickness, which indicated the presence of a 'bubble' near the flame tip. The further analysis of these statistics in the LES conducted by Langella et al. (2016a) indicated that the LES modelling with a presumed PDF approach was not capable of predicting such behaviours even with a mesh of 20 million elements. It was argued that for the velocity field to exhibit bimodality, the flame has to quickly move around the probing point. Consequently, the LES in Langella et al. (2016a) did not predict it either because the amplitude and speed of the flame movement in the radial direction was not captured accurately, or because a much finer mesh was required. Also, no 'bubble' was observed in the LES. A further investigation conducted on LES data in the current study, however, indicates the presence of vortex rings forming at the nozzle exit due to the boundary layer detachment and interaction with the flame near the anchoring point, where stretch and heat loss effect might be influencing the flame dynamics. These vortices bring vorticity that travels downstream in the quasi-laminar region before being suppressed by thermal dilatation effects and it is possible that they affect the flame

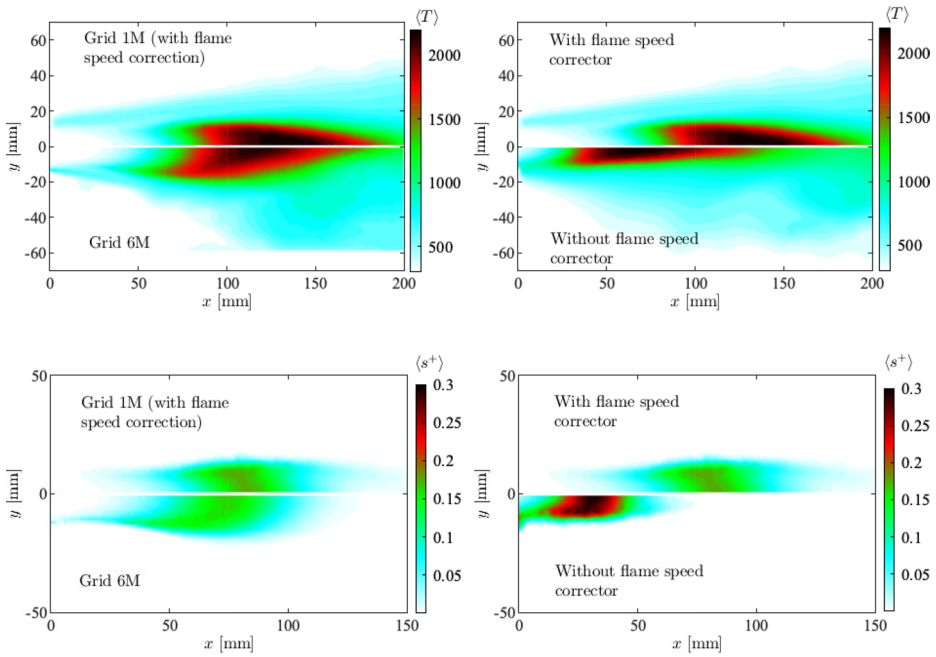

Fig. 6 Contours of mean temperature (top) and mean s^+ (bottom) obtained from LES using the 6 M grid and the 1 M grid with and without flame speed correction

movement in the radial direction, which is something that could not be studied in Langella et al. (2016a) where the nozzle was not within the numerical domain. Nevertheless, since these ring vortices also cause some mixing with air in the region immediately near the flame anchoring point, their study in the context of the fully premixed model under investigation here would not be fully appropriate. Also, although such an investigation would certainly be of interest, it goes beyond the purpose of this work, where only a reference flame is needed for the fully premixed, unstrained flamelet model. It is worth noting that, due to the reasons above, the use of a fully premixed model would not fully capture the vortex-flame interplay near the anchoring point as the flame is not fully premixed in that region. As this behaviour is linked to that of the radial velocity profiles, further experimental data available in 9 are not discussed here and this is left for future work, where the physics near the anchoring point can be better investigated also in the context of possible stretch and heat losses effects. Nevertheless, this is not relevant for the analysis in the next section, namely demonstrating the effectiveness of the flame consumption speed correction discussed in Sect. 3. Indeed, the spurious increase of consumption speed can be verified just by the comparison of the numerical simulations on different grids.

To provide further insights, the consumption speed s_c is compared for the 6 M and 1 M grids with and without using the flame speed correction. A local consumption speed in the LES can be defined according to the product-based progress variable as

$$s_c = \frac{1}{\Psi^b \rho^b} \int_{\mathcal{V}} \overline{\dot{\omega}}_c \, d\mathcal{V} \tag{10}$$

Given the consumption speed is an extensive quantity and is volume-dependent, in order to compare results for the two grids, a normalised speed is derived by dividing s_c by the local cell volume. Considering Eq. (7), this normalised reaction rate becomes $s^+ = f(\Delta)\overline{\dot{\omega}}_c \delta_{th}/(\rho^b s_L)$, where $f(\Delta) = 1$ for the 6 M grid and is either 1 or taken from Eq. (7) on the 1 M grid depending on whether the flame speed corrector is used. Note that this quantity is meant here to represent a flame speed rather than a reaction rate. Contours of time averaged s^+ are shown in Fig. 6 (bottom). A reasonable agreement between s^+ is obtained between the 6 M and the 1 M grids when the correction $f(\Delta)$ is used, which explains why the flame remains in the same position. More in detail, the flame length seems to be reasonably well recovered, while some discrepancy is still observed in terms of flame width. On the contrary, values twice as strong are found for the 1 M grid, which explains its positioning upstream where local flow rates are higher.

The scatter plots of Fig. 7 show the behaviour of (normalised) reaction rate conditioned on progress variable for the two grids. These scatter plots help to understand the behaviour of the reaction rate as it is obtained from the flamelet table. For a certain value of $\widetilde{c}$, this depends on the value of SGS variance, which is shown in colours in the plots. First, one can observe that the values of conditional reaction rate are larger for the 1 M grid in the case without correction, which reflects the fact that the flame is positioned in a region of higher reactant velocities and thus higher reaction rates are required. It is worth noting that the mesh is nearly uniform in the region of the flame as can be observed from Fig. 4. Values of conditional SGS variance shown in Fig. 7d for the 1 M grid cases with and without correction are also similar, suggesting that the higher reaction rates are a result of a decreased variance at the LES resolved level. In fact, the resolved variance is observed to decrease by

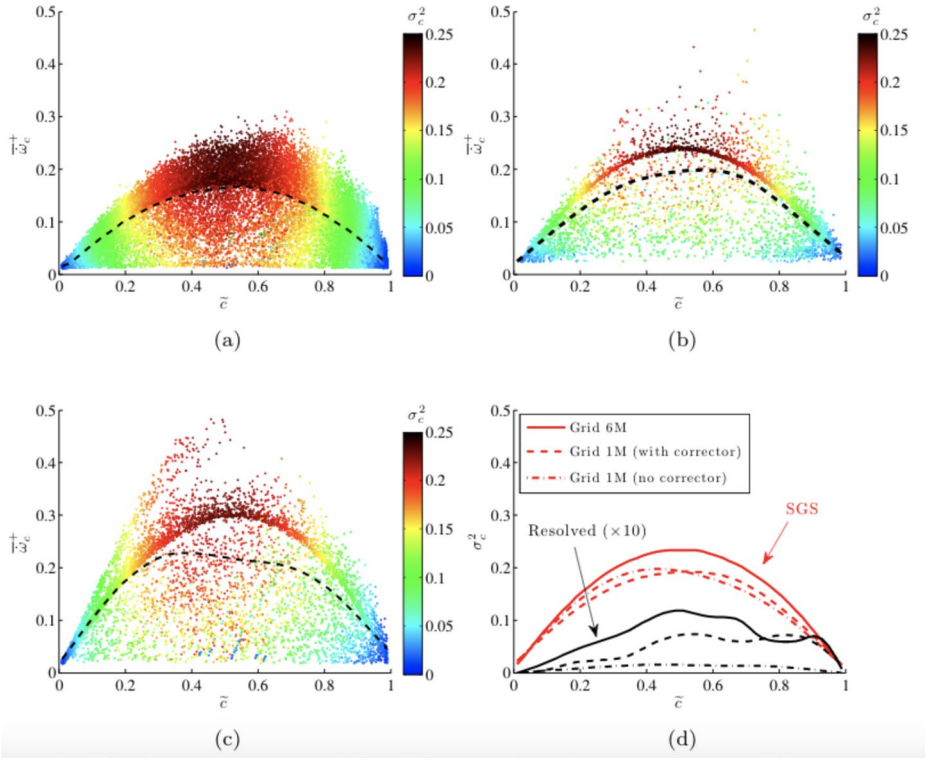

Fig. 7 Scatter plots, coloured by SGS variance, of normalised reaction rate, $\overline{\dot{\omega}}_c^+ = \overline{\dot{\omega}}_c \delta_{th}/(\overline{\rho} s_L)$ for the (**a**) 6 M, and (**b**) 1 M grids with and (**c**) without flame speed correction. Dashed line indicate the conditional averages. (**d**) Conditional averages for SGS and resolved variance of $\widetilde{c}$

a factor of 5, from about 0.01 in the correct flame position, to 0.002 in the shorter flame. Although both values are relatively low compared to the respective SGS values (combustion is at SGS level on these grids), this difference is sufficient to yield the observed mean reaction rate behaviour. It is worth noting that the high values of SGS variances observed are a consequence of the strong reactive term in the variance equation and a relatively low scatter at fixed values of $\widetilde{c}$. Further considerations on the SGS variance are given in Sect. 4.3.

4.3 Further Considerations on the SGS Variance

The SGS variance behaviour in Fig. 7d can be counter-intuitive as lower values are observed for the coarser mesh. When the flame speed correction is not used, this is simply a consequence of the flame stabilising in a different position. As the correction model only affects the burning speed and not the variance, however, the variance value does not come back to the values observed for the 6 M grid. This poses questions on the meaning of the SGS variance, which is due to the fact that this variance is a controlling parameter in presumed PDF approaches. One could in fact equivalently increase the SGS variance magnitude by tuning the SDR model constant. The fundamental question is whether the right value of σ_c^2 is the one observed after applying the flame speed correction, or the one, one would obtain

by varying the subgrid SDR model constants. As discussed in Sect. 3, the SGS variance obtained using the flame speed correction is physically related to the consumption speed, and thus may be a better candidate to represent the actual subgrid fluctuation level of $\widetilde{c}$. Indeed, the only leading term for SGS variance generation in Eq. (3) is the reactive term $\mathcal{R} \gg \mathcal{P}$ in quasi-laminar configurations, which was shown to be well estimated in a priori analyses also for $\Delta > \delta_{th}$ (Nilsson et al., 2019a). Also, applying the same correction of Eq. (7) to $\mathcal{R}$ would imply altering the balance between $\mathcal{R}$, $\mathcal{P}$ and SDR in premixed combustion, and this coupling was not accounted for in the a priori analysis by 27. A sensitivity study was conducted here by applying the correction of Eq. (7) to the reactive term $\mathcal{R}$. Results (not shown) showed indeed only a partial recovery of the flame length, which may partly be due to the subgrid SDR model not fully taking into account the revised balance. Further a priori analyses are thus needed to shed light on the significance of SGS variance in LES and its interlink to SDR, FDF and reaction rate.

5 Conclusions

The relation between FDF, SGS variance and reaction rate is investigated *a posteriori* in light of a novel correction for the burning speed in the context of presumed FDF approach with β function. It is first shown that this correction is generalisable to partially premixed conditions and that the generalised form has weak dependence on fuel and operative conditions, at least at lean conditions. Large eddy simulations of a premixed quasi-laminar jet flame combustion have then been presented to assess the performance of the flame speed correction. The β-PDF is in particular known to overestimate the reaction rate under quasi-laminar conditions. This behaviour is discussed in this work and related to an incorrect prediction of the SGS variance by the β-PDF for cases where the filter width is larger than the laminar flame thickness. The model tested in this work shows the ability to recover the correct flame speed behaviour without directly affecting the SGS variance. In principle, this correction can be applied to any flamelet-like model such as the Flamelet Generated Manifold to ensure that the consumption speed is correctly predicted when a presumed-FDF approach is applied. However, additional tests are need to understand the significance of the SGS variance in LES.

Acknowledgements The authors would also like to acknowledge Dr. M. P. Sitte for useful suggestions.

Author Contributions Both authors contributed to the study conception and design. Material preparation and data collection were performed by Ivan Langella. The analysis and the first draft of the manuscript were done jointly by the authors and both authors commented on previous versions of the manuscript. Both authors read and approved the final manuscript.

Funding The authors did not receive support from any organization for the submitted work.

Data Availability No datasets were generated or analysed during the current study.

Declarations

Competing Interests The authors declare no competing interests.

References

Bray, K.: Laminar flamelets in turbulent combustion modeling. Combust. Sci. Technol. **188**(9), 1372–1375 (2016). https://doi.org/10.1080/00102202.2016.1195819

Chai, X., Mahesh, K.: Dynamic -equation model for large-eddy simulation of compressible flows. J Fluid Mech. **699**, 385–413 (2012). https://doi.org/10.1017/jfm.2012.115

Doan, N.A.K., Swaminathan, N., Chakraborty, N.: Multiscale analysis of turbulence-flame interaction in premixed flames. Proc. Combust. Inst. **36**(2), 1929–1935 (2017). https://doi.org/10.1016/j.proci.2016.07.111

Donini, A., Bastiaans, R.J.M., Oijen, J.A., Goey, L.P.H.: A 5-D implementation of FGM for the large eddy simulation of a stratified swirled flame with heat loss in a gas turbine combustor. Flow Turbul. Combust. **98**(3), 887–922 (2017). https://doi.org/10.1007/s10494-016-9777-7

Dunstan, T.D., Minamoto, Y., Chakraborty, N., Swaminathan, N.: Scalar dissipation rate modelling for large eddy simulation of turbulent premixed flames. Proc. Combust. Inst. **34**(1), 1193–1201 (2013). https://doi.org/10.1016/j.proci.2012.06.143

Fiorina, B., Baron, R., Gicquel, O., Thevenin, D., Carpentier, S., Darabiha, N.: Modelling non-adiabatic partially premixed flames using flame-prolongation of ILDM. Combust. Theor. Model. **7**(3), 449–470 (2003). https://doi.org/10.1088/1364-7830/7/3/301

Fiorina, B., Veynante, D., Candel, S.: Modeling combustion chemistry in large eddy simulation of turbulent flames. Flow Turbul. Combust. **94**(1), 3–42 (2015). https://doi.org/10.1007/s10494-014-9579-8

Fiorina, B., Vicquelin, R., Auzillon, P., Darabiha, N., Gicquel, O., Veynante, D.: A filtered tabulated chemistry model for les of premixed combustion. Combust Flame **157**(3), 465–475 (2010). https://doi.org/10.1016/j.combustflame.2009.09.015

Furukawa, J., Yoshida, Y., Williams, F.A.: Structures of methane-air and propane-air turbulent premixed Bunsen flames. Combust. Sci. Technol. **188**(9), 1538–1564 (2016). https://doi.org/10.1080/00102202.2016.1198335

Galeazzo, F.C.C., Savard, B., Wang, H., Hawkes, E.R., Chen, J.H., Filho, G.C.K.: Performance assessment of flamelet models in flame-resolved les of a high karlovitz methane/air stratified premixed jet flame. Proc. Combust. Inst. **37**(2), 2545–2553 (2019). https://doi.org/10.1016/j.proci.2018.09.025

Gicquel, L.Y.M., Staffelbach, G., Poinsot, T.: Large eddy simulations of gaseous flames in gas turbine combustion chambers. Prog Energy Combust Sci. **38**(6), 782–817 (2012). https://doi.org/10.1016/j.pecs.2012.04.004

Jarrin, N., Benhamadouche, S., Laurence, D., Prosser, R.: A synthetic-eddy-method for generating inflow conditions for large-eddy simulations. Int J Heat Fluid Flow **27**(4), 585–593 (2006). https://doi.org/10.1016/j.ijheatfluidflow.2006.02.006

Kee, R.J., Grcar, J.F., Smooke, M.D., Miller, J.A.: A Fortran Program for Modeling Steady Laminar One-Dimensional Premixed Flames. Report No. SAND85-8240, Sandia National Labortories, CA, USA (1985)

Klapdor, E.V., Mare, F., Kollmann, W., Janicka, J.: A compressible pressure-based solution algorithm for gas turbine combustion chambers using the pdf/fgm model. Flow Turbul. Combust. **91**(2), 209–247 (2013). https://doi.org/10.1007/s10494-013-9451-2

Klein, M., Chakraborty, N., Pfitzner, M.: Analysis of the combined modelling of sub-grid transport and filtered flame propagation for premixed turbulent combustion. Flow Turbul. Combust. **96**(4), 921–938 (2016). https://doi.org/10.1007/s10494-016-9714-9

Klein, M., Sadiki, A., Janicka, J.: A digital filter based generation of inflow data for spatially developing direct numerical or large eddy simulations. J. Comput. Phys. **186**(2), 652–665 (2003). https://doi.org/10.1016/S0021-9991(03)00090-1

Kravchenko, A., Moin, P.: Numerical studies of flow over a circular cylinder at re_d = 3900. Phys. Fluids **12**, 403–417 (2000)

Langella, I., Doan, N.A.K., Swaminathan, N., Pope, S.B.: Study of subgrid-scale velocity models for reacting and nonreacting flows. Phys. Rev. Fluids. **3**(5) (2018). https://doi.org/10.1103/PhysRevFluids.3.054602

Langella, I., Swaminathan, N.: Unstrained and strained flamelets for LES of premixed combustion. Combust. Theor. Model. **20**(3), 410–440 (2016). https://doi.org/10.1080/13647830.2016.1140230

Langella, I., Swaminathan, N., Pitz, R.W.: Application of unstrained flamelet SGS closure for multi-regime premixed combustion. Combust Flame **173**, 161–178 (2016a). https://doi.org/10.1016/j.combustflame.2016.08.025

Langella, I., Swaminathan, N., Williams, F.A., Furukawa, J.: Large-eddy simulation of premixed combustion in the corrugated-flamelet regime. Combust. Sci. Technol. **188**(9), 1565–1591 (2016b). https://doi.org/10.1080/00102202.2016.1195824

Lecocq, G., Richard, S., Colin, O., Vervisch, L.: Hybrid presumed pdf and flame surface density approaches for large-eddy simulation of premixed turbulent combustion: part 1: formalism and simulation of a quasi-steady burner. Combust Flame **158**(6), 1201–1214 (2011). https://doi.org/10.1016/j.combustflame.2010.09.023

Lee, S., Lele, S.K., Moin, P.: Simulation of spatially evolving turbulence and the applicability of Taylor's hypothesis in compressible flow. Phys. Fluids **4**(7), 1521–1530 (1992). https://doi.org/10.1063/1.858425

Lipatnikov, A.N., Sabelnikov, V.A., Hernández-Pérez, F.E., Song, W., Im, H.G.: Prediction of mean radical concentrations in lean hydrogen-air turbulent flames at different karlovitz numbers adopting a newly extended flamelet-based presumed PDF. Combust Flame **226**, 248–259 (2021). https://doi.org/10.1016/j.combustflame.2020.12.009

Meyers, J., Sagaut, P.: Is plane-channel flow a friendly case for the testing of large-eddy simulation subgrid-scale models? Phys. Fluids **19**(4), 048105 (2007). https://doi.org/10.1063/1.2722422

Nilsson, T., Langella, I., Doan, N.A.K., Swaminathan, N., Yu, R., Bai, X.-S.: A priori analysis of sub-grid variance of a reactive scalar using dns data of high ka flames. Combust. Theor. Model. **23**(5), 885–906 (2019a). https://doi.org/10.1080/13647830.2019.1600033

Nilsson, T., Yu, R., Doan, N.A.K., Langella, I., Swaminathan, N., Bai, X.-S.: Filtered reaction rate modelling in moderate and high karlovitz number flames: an *a priori* analysis. Flow Turbul. Combust. **103**(3), 643–665 (2019b). https://doi.org/10.1007/s10494-019-00038-8

Pfitzner, M.: A new analytic pdf for simulations of premixed turbulent combustion. Flow Turbul. Combust. **106**(4), 1213–1239 (2021). https://doi.org/10.1007/s10494-020-00137-x

Piomelli, U., Balaras, E.: Wall-layer models for large-eddy simulations. Annu Rev Fluid Mech. **34**(1), 349–374 (2002). https://doi.org/10.1146/annurev.fluid.34.082901.144919

Pope, S.B.: Turbulent Flows. Cambridge University Press, ??? (2000)

Ribert, G., Champion, M., Plion, P.: Modeling turbulent reactive flows with variable equivalence ratio: application to the calculation of a reactive shear layer. Combust. Sci. Technol. **176**(5–6), 907–923 (2004). https://doi.org/10.1080/00102200490428530

Salehi, M.M., Bushe, W.: Presumed PDF modeling for RANS simulation of turbulent premixed flames. Combust. Theor. Model. **14**(3), 381–403 (2010). https://doi.org/10.1080/13647830.2010.489957

Salehi, M.M., Bushe, W.K., Shahbazian, N., Groth, C.P.T.: Modified laminar flamelet presumed probability density function for LES of premixed turbulent combustion. Proc. Combust. Inst. **34**(1), 1203–1211 (2013). https://doi.org/10.1016/j.proci.2012.06.177

Soli, A., Langella, I., Chen, Z.X.: Analysis of flame front breaks appearing in les of inhomogeneous jet flames using flamelets. Flow Turbul. Combust. **108**(4), 1159–1190 (2022). https://doi.org/10.1007/s10494-021-00306-6

Trisjono, P., Kleinheinz, K., Pitsch, H., Kang, S.: Large eddy simulation of stratified and sheared flames of a premixed turbulent stratified flame burner using a flamelet model with heat loss. Flow Turbul. Combust. **92**(1–2), 201–235 (2014). https://doi.org/10.1007/s10494-013-9522-4

van Oijen, J.A., Donini, A., Bastiaans, R.J.M., Thije Boonkkamp, J.H.M., Goey, L.P.H.: State of-the-art in premixed combustion modeling using flamelet generated manifolds. Prog Energy Combust Sci. **57**, 30–74 (2016)